Pseudocompressible approximation and statistical turbulence modeling: Application to shock tube flows

Olivier Soulard,* Jérôme Griffond, and Denis Souffland
CEA, DAM, DIF, F-91297 Arpajon, France

(Received 4 August 2011; revised manuscript received 6 December 2011; published 8 February 2012)

In this work, a pseudocompressible approximation relevant for turbulent mixing flows encountered in shock tubes is derived. The asymptotic analysis used for this purpose puts forward the role played by four dimensionless numbers on the flow compressibility, namely, the turbulent, deformation, stratification, and buoyancy force Mach numbers. The existence of rapid distortion and diffusion-dissipation regimes is also accounted for in the analysis. Some consequences of the derived pseudocompressible approximation on statistical turbulence models are discussed. In particular, the evolutions of the density variance and flux are examined, as well as the turbulent transport of energy. The different aspects of this study are assessed by performing a direct numerical simulation of a shock tube flow configuration.

DOI: 10.1103/PhysRevE.85.026307 PACS number(s): 47.27.eb, 47.27.ek, 47.27.em, 47.27.wj

I. INTRODUCTION

The asymptotic analysis of low-Mach-number flows, for which the instantaneous fluid velocity is small compared to the sound speed, plays a significant role in a wide variety of fields, ranging from geophysical flows (ocean and atmosphere [1–3]) to engine combustion (aeronautics and automotive industry [4]), supernova explosions [5–7], or inertial confinement fusion experiments [8]. The main purpose of these asymptotic analyses is to formulate an approximation of the real flow that allows one to filter out acoustical phenomena. Depending on their field of application and their range of validity, these approximations are referred to in several ways: low-Mach, anelastic, quasicompressible or pseudocompressible, quasi-isobaric, Boussinesq, Boussinesq-Oberbeck, etc. We will hereafter use pseudocompressible as a generic term referring to all of these approximations.

Pseudocompressible approximations can have very different expressions depending on the context in which they are applied. However, they usually share two common points. First, the pressure fluctuations relative to a given deterministic reference state become negligible with respect to velocity fluctuations and/or fluctuations of other thermodynamic quantities. In contrast, the fluctuating pressure gradient plays an important role and cannot be neglected. Second, the velocity divergence can be related to the evolution of the said deterministic reference state. This relationship allows one to derive from the momentum equation a Poisson equation for the fluctuating pressure.

These properties of pseudocompressible approximations have a deep impact on the formulation of statistical turbulence models. For instance, most closures for the fluctuating pressure gradient used in second order [9] or probability density function models [10,11] are derived by using the previously mentioned Poisson equation. Furthermore, for variable density turbulent flows, the relationship to the velocity divergence allows for an explicit treatment of some compressibility effects. These effects can then be taken into account in a model without any additional closure [12,13]. Finally, as the pressure fluctuations are negligible, the derivation of a statistical model only requires the description of the statistics of the remaining thermodynamical quantities (e.g., density and concentrations) to correctly predict the turbulent flow even if it is compressible and density variable.

The consequences of pseudocompressible approximations on statistical turbulence models have been studied in detail in many fields [11–15]. However, it seems that no analysis has been dedicated to variable density turbulent mixing flows encountered in shock tubes. Andronov *et al.* [16] explicitly used a pseudo-compressible-like hypothesis when they derived their second-order model. Nevertheless, their approach remains semiempirical and does not clarify the origin and the validity of their approximations.

The primary reason for this lack of investigation comes from some specificities of shock tube flows that are unaccounted for in usual pseudocompressible approximations. First, the reference state about which the asymptotic analysis is derived is neither static [1] nor obeying a pseudocompressible approximation [6]: It is strongly compressible and depends on space and time. Second, density fluctuations due to species mixing as well as polytropic index fluctuations must be taken into account. The amplitudes of these fluctuations are non-negligible with respect to their mean values. Third, the fluids are not necessarily perfect gases and their equations of state play a crucial role [17]. Finally, the compression or rarefaction waves traveling in shock tube flows can induce regimes of rapidly distorted turbulence (RDT) [18]. This point is important since it has been shown [19–22] that mean flow deformations in the RDT regime modify the compressibility properties of the flow and may invalidate pseudocompressible approximations. In shock tubes, the RDT regime results from the action of baroclinic forces rather than from mean flow deformations. The effect of these forces in the RDT regime on the pseudocompressible approximation and its validity does not seem to have been thoroughly studied and requires some precision.

Thus, the purpose of this work is first to derive a pseudocompressible approximation relevant to turbulent mixing flows encountered in shock tubes, that is to say, accounting

*olivier.soulard@cea.fr

for the specificities described above, and then to examine the consequences of this approximation on some properties of statistical turbulence models used for predicting shock tube flows. To this aim, we first proceed to an asymptotic analysis based on the evolutions of the fluctuations of velocity, density, and pressure. From this analysis, four dimensionless numbers are shown to play a role in the flow compressibility: the turbulent Mach number, the deformation Mach number, the stratification Mach number, and the buoyancy force Mach number. We show that the asymptotic developments are different depending on whether or not the flow evolves under RDT conditions. Indeed, the validity conditions and the order of the fluctuating pressure are not the same depending on the considered regime. Despite these differences, a single expression of the fluctuating velocity divergence that is valid in the pseudocompressible limit for both regimes.

We then illustrate the implications of the pseudocompressible approximation on turbulence modeling by considering second-order one-point turbulence models dedicated to shock tube flows [23–26]. We show that the pseudocompressible approximation allows one to specify unambiguously some production terms appearing in the evolution equations of the density variance and density flux of these models. In addition, the pseudocompressible approximation also leads to a direct closure of the turbulent transport term appearing in the mean energy equation.

These results are evaluated by comparison with a numerical simulation of a shock tube flow. This simulation includes a diffusion-dissipation phase and a countergradient transport phase resulting from the interaction with a rarefaction wave.

II. FLOW DESCRIPTION

A. Instantaneous equations

We consider a flow state that is defined by its density ρ, velocity $\boldsymbol{U}$, internal energy e, and species mass fractions $\{Y_\alpha,\ \alpha = 1,\ldots,N_s\}$. These variables evolve according to Navier-Stokes equations [27]

$$\frac{\partial \rho}{\partial t} + U_j \frac{\partial \rho}{\partial x_j} = -\rho \boldsymbol{\nabla}\cdot\boldsymbol{U}, \tag{1}$$

$$\frac{\partial U_i}{\partial t} + U_j \frac{\partial U_i}{\partial x_j} = -\frac{1}{\rho}\frac{\partial P}{\partial x_i} - \frac{1}{\rho}\frac{\partial \sigma_{ij}}{\partial x_j}, \tag{2}$$

$$\frac{\partial e}{\partial t} + U_j \frac{\partial e}{\partial x_j} = \varepsilon - \frac{P}{\rho}\boldsymbol{\nabla}\cdot\boldsymbol{U} - \frac{1}{\rho}\frac{\partial \mathcal{Q}_j}{\partial x_j}, \tag{3}$$

$$\frac{\partial Y_\alpha}{\partial t} + U_j \frac{\partial Y_\alpha}{\partial x_j} = -\frac{1}{\rho}\frac{\partial \mathcal{F}_j^\alpha}{\partial x_j}, \tag{4}$$

where P is the pressure, σ_{ij} is the viscosity tensor, $\mathcal{F}_j^\alpha$ is the molecular diffusion flux of scalar α, and $\mathcal{Q}_j$ is the molecular heat flux. The viscous dissipation rate ε is defined as $\rho\varepsilon = -\sigma_{ij}S_{ji}$, where S_{ij} is the instantaneous strain-rate tensor $S_{ij} = (\partial U_i/\partial x_j + \partial U_j/\partial x_i)/2$. For the sake of conciseness, the velocity divergence $\partial U_j/\partial x_j$ is denoted by $\boldsymbol{\nabla}\cdot\boldsymbol{U}$, with the help of the nabla operator.

We assume that the pressure is a function of density, energy, and mass fractions

$$P \equiv P(\rho, e, \boldsymbol{Y}). \tag{5}$$

This function is supposed to be differentiable. Then, the pressure evolution is derived by differentiating Eq. (5) with respect to time and by substituting Eqs. (1)–(4) into the resulting expression. After using some of Maxwell's thermodynamical relations, one obtains

$$\frac{\partial P}{\partial t} + U_j \frac{\partial P}{\partial x_j} = -\gamma_1 P \boldsymbol{\nabla}\cdot\boldsymbol{U} + \mathcal{D}_p, \tag{6}$$

with

$$\mathcal{D}_p = (\gamma_3 - 1)\left[\rho\varepsilon - \frac{\partial \mathcal{Q}_j}{\partial x_j} + h_\alpha \frac{\partial \mathcal{F}_j^\alpha}{\partial x_j}\right] + \gamma_3 P_\alpha \left[-\frac{1}{\rho}\frac{\partial \mathcal{F}_j^\alpha}{\partial x_j}\right], \tag{7}$$

$$\gamma_1 = \frac{\rho}{P}\left.\frac{\partial P}{\partial \rho}\right|_{\mathtt{s},\boldsymbol{Y}} = \frac{\rho}{P}a^2, \quad \gamma_3 = 1 + \frac{1}{\rho}\left.\frac{\partial P}{\partial e}\right|_{\rho,\boldsymbol{Y}}, \tag{8}$$

$$P_\alpha = \left.\frac{\partial P}{\partial Y_\alpha}\right|_{\rho,T,\boldsymbol{Y}\neq Y_\alpha}, \quad h_\alpha = \left.\frac{\partial h}{\partial Y_\alpha}\right|_{\rho,T,\boldsymbol{Y}\neq Y_\alpha}, \tag{9}$$

where $\mathtt{s}$ is the entropy, h is the enthalpy, a is the sound speed, and T is the temperature. The quantities P_α and h_α play the role of a pressure and an enthalpy specific to the scalar α. The generalized polytropic indices γ_1 and γ_3 are introduced in Refs. [28,29]. In a perfect gas, γ_1 and γ_3 are equal to the ratio γ of the constant pressure specific heat C_p to the constant volume specific heat C_v:

$$\gamma = \frac{C_p}{C_v}, \quad C_v = \left.\frac{\partial e}{\partial T}\right|_{\rho,\boldsymbol{Y}}, \quad C_p = \left.\frac{\partial h}{\partial T}\right|_{P,\boldsymbol{Y}}.$$

However, in the general case, $\gamma \neq \gamma_1 \neq \gamma_3$. To conclude the flow description, we give expressions for the molecular transport fluxes that are valid at least in the case of perfect gases [27]:

$$\sigma_{ij} = -\kappa \boldsymbol{\nabla}\cdot\boldsymbol{U}\delta_{ij} - 2\eta\left(S_{ij} - \tfrac{1}{3}\boldsymbol{\nabla}\cdot\boldsymbol{U}\delta_{ij}\right), \tag{10}$$

$$\mathcal{F}_j^\alpha = -\rho\mathcal{D}^{(\alpha)}\frac{\partial Y_\alpha}{\partial x_j} \quad \text{for } \alpha = 1,\ldots,N_s - 1,$$

$$\mathcal{F}_j^{N_s} = -\sum_{\alpha=1}^{N_s-1}\mathcal{F}_j^\alpha, \tag{11}$$

$$\mathcal{Q}_j = -\lambda\frac{\partial T}{\partial x_j} + \sum_\alpha h_\alpha \mathcal{F}_j^\alpha, \tag{12}$$

where λ is the thermal conductivity, κ and η are the bulk and shear viscosity of the fluid, and $\mathcal{D}^{(\alpha)}$ is the diffusion of the scalar α in a Fickian approximation.

B. Dimensionless equations for the fluctuations

The goal of this section is to make dimensionless the evolution equations for the fluctuation of velocity $\boldsymbol{U}''$, density ρ', and pressure P'. The key parameters acting on the compressibility of the turbulent field are thus presented.

We remind the reader that for variable density flows, it is usual to work with both Favre (density weighted) and Reynolds (unweighted) statistics. Reynolds and Favre averages of a quantity Q are respectively denoted by $\overline{Q}$ and $\widetilde{Q}$ and are linked by the identity $\widetilde{Q} = \overline{\rho Q}/\overline{\rho}$. Reynolds and Favre fluctuations

are respectively denoted by Q' and Q'' and are related by $Q'' = \overline{Q''} + Q'$.

Dimensional equations for $\boldsymbol{U}''$, ρ', and P' are straightforwardly obtained from Eqs. (1), (2), and (6) with classical techniques [15]. We directly introduce their dimensionless formulations, which are useful for the asymptotic study; however, first, we need to define characteristic scales for fluctuating quantities as well as for mean quantities, mean gradients, and finally space and time.

1. Characteristic scales

Let v, ϱ, and Υ be the characteristic scales of the fluctuations of velocity $\boldsymbol{U}''$, density ρ', and polytropic index γ_1'. Let also ρ_0, P_0, and γ_{10} be the mean scales of density, pressure, and index γ_1. Then, the characteristic sound speed is $a_0 = \sqrt{\gamma_{10} P_0/\rho_0}$. Furthermore, let G_0 be the scale of mean acceleration, S_0 that of the mean strain rate, and L_0 that of the mean density gradient. Finally, let ℓ denote the characteristic spatial scale of the turbulent field and t_0 the temporal scale of the flow. The time t_0 is not necessarily equal to the turbulent time defined as $\tau = \ell/\mathrm{v}$.

The corresponding dimensionless quantities are

$$t^* = \frac{t}{t_0}, \quad \boldsymbol{x}^* = \frac{\boldsymbol{x}}{\ell}, \quad \boldsymbol{u}''^* = \frac{\boldsymbol{U}''}{\mathrm{v}}, \quad \rho'^* = \frac{\rho'}{\varrho}, \quad \gamma_1'^* = \frac{\gamma_1'}{\Upsilon},$$

$$p'^* = \frac{P'}{P_0}, \quad \overline{\rho}^* = \frac{\overline{\rho}}{\rho_0}, \quad \overline{P}^* = \frac{\overline{P}}{P_0}, \quad \overline{\gamma}_1^* = \frac{\overline{\gamma}_1}{\gamma_{10}},$$

$$\left.\frac{1}{\overline{\rho}}\frac{\partial \overline{P}}{\partial x_i}\right|^* = \frac{1}{G_0}\frac{1}{\overline{\rho}}\frac{\partial \overline{P}}{\partial x_i}, \quad \left.\frac{\partial \widetilde{U}_i}{\partial x_j}\right|^* = \frac{1}{S_0}\frac{\partial \widetilde{U}_i}{\partial x_j},$$

$$\left.\frac{1}{\overline{\rho}}\frac{\partial \overline{\rho}}{\partial x_i}\right|^* = L_0\frac{1}{\overline{\rho}}\frac{\partial \overline{\rho}}{\partial x_i}.$$

Notice that P' is not nondimensionalized in the same way as other fluctuating variables. Indeed, in the asymptotic analysis, the order of ρ', γ_1', and $\boldsymbol{U}''$ is imposed by hypotheses, whereas the order of P' is deduced from analysis.

Molecular transport terms do not play an important role in the asymptotic analysis, so a simplified approach is used to make them dimensionless. Let η_0 be a characteristic dynamic viscosity and Pr a characteristic Prandtl number of the flow. We assume that molecular transport terms can be nondimensionalized with

$$\sigma_{ij}^* = \frac{\ell}{\mathrm{v}\eta_0}\sigma_{ij}, \quad \mathcal{D}_p^* = \frac{\rho_0 \ell^2}{P_0}\frac{\mathrm{Pr}}{\eta_0}\frac{\rho_0}{\varrho}\mathcal{D}_p.$$

2. Dimensionless equations

For the sake of simplicity, the asterisk superscripts are dropped in the following. With this convention, the dimensionless equations for $\boldsymbol{U}''$, ρ', and P' are

$$\frac{1}{\xi}\frac{D\rho'}{Dt} = -\left[\frac{1}{\epsilon_\varrho}\right]\rho\nabla\cdot\boldsymbol{u'} - \left[\frac{\mathtt{M_n^2}}{\mathtt{M_a M_t}}\right]u_j''\frac{\partial\overline{\rho}}{\partial x_j} - \left[\frac{\mathtt{M_s}}{\mathtt{M_t}}\right]\rho'\nabla\cdot\overline{\boldsymbol{U}} - \overline{\rho}\nabla\cdot\overline{\boldsymbol{u}}'', \tag{13}$$

$$\frac{1}{\xi}\frac{Du_i''}{Dt} = -\left[\frac{1}{\gamma_{10}\mathtt{M_t^2}}\right]\frac{1}{\rho}\frac{\partial p'}{\partial x_i} - \left[\frac{\mathtt{M_s}}{\mathtt{M_t}}\right]u_j''\frac{\partial\widetilde{U}_i}{\partial x_j} + \left[\frac{\mathtt{M_a}}{\mathtt{M_t}}\right]\frac{\rho'}{\rho\overline{\rho}}\frac{\partial\overline{P}}{\partial x_i} + \frac{1}{\overline{\rho}}\frac{\partial}{\partial x_j}(\overline{\rho}\widetilde{u_i''u_j''}) - \left[\frac{1}{\mathrm{Re}_t}\right]\left\{\frac{1}{\rho}\frac{\partial\sigma_{ij}'}{\partial x_j} - \epsilon_\varrho\frac{\rho'}{\rho\overline{\rho}}\frac{\partial\overline{\sigma}_{ij}}{\partial x_j}\right\}, \tag{14}$$

$$\begin{aligned}\frac{1}{\xi\gamma_{10}}\frac{Dp'}{Dt} = &-\overline{\gamma}_1\overline{P}\nabla\cdot\boldsymbol{u'} - \left[\frac{\mathtt{M_a M_t}}{\epsilon_\varrho}\right]u_j'\frac{\partial\overline{P}}{\partial x_j} \\ &- \left[\frac{\epsilon_\gamma\mathtt{M_s}}{\mathtt{M_t}}\right]\gamma_1'\overline{P}\nabla\cdot\overline{\boldsymbol{U}} - \left[\frac{\mathtt{M_s}}{\mathtt{M_t}}\right]\overline{\gamma}_1 p'\nabla\cdot\overline{\boldsymbol{U}} \\ &-[\epsilon_\gamma](\gamma_1'\nabla\cdot\boldsymbol{u'} - \overline{\gamma_1'\nabla\cdot\boldsymbol{u'}})\overline{P} \\ &- \left[\frac{\epsilon_\gamma\mathtt{M_s}}{\mathtt{M_t}}\right](\gamma_1'p' - \overline{\gamma_1'p'})\nabla\cdot\overline{\boldsymbol{U}} \\ &-\overline{\gamma}_1(p'\nabla\cdot\boldsymbol{u'} - \overline{p'\nabla\cdot\boldsymbol{u'}}) \\ &-[\epsilon_\gamma](\gamma_1'p'\nabla\cdot\boldsymbol{u'} - \overline{\gamma_1'p'\nabla\cdot\boldsymbol{u'}}) \\ &-\frac{1}{\gamma_{10}}\overline{p'\nabla\cdot\boldsymbol{u'}} + \frac{1}{\gamma_{10}}\frac{\partial}{\partial x_j}(\overline{p'u_j'}) + \frac{\epsilon_\varrho}{\mathrm{Pr}\,\mathrm{Re}_t}\mathcal{D}_p'.\end{aligned} \tag{15}$$

Three dimensionless numbers characterize the turbulent fluctuations intensity: the turbulent Mach number and the ratios of fluctuations to averages of density ϵ_ϱ and polytropic index ϵ_γ. They are defined as

$$\mathtt{M_t} = \frac{\mathrm{v}}{a_0}, \quad \epsilon_\varrho = \frac{\varrho}{\rho_0}, \quad \epsilon_\gamma = \frac{\Upsilon}{\gamma_{10}}.$$

Furthermore, three other numbers characterize the interaction between the mean fields and the turbulent field. These Mach numbers are related to the strain, the stratification, and the acceleration:

$$\mathtt{M_s} = \frac{S_0\ell}{a_0}, \quad \mathtt{M_n} = \frac{N_0\ell}{a_0}, \quad \mathtt{M_a} = \frac{A_0\ell}{a_0},$$

where N_0 is the Brunt-Väisällä frequency and A_0 is the buoyancy force frequency:

$$N_0 = \sqrt{\left|\frac{G_0}{L_0}\right|}, \quad A_0 = \frac{G_0\epsilon_\varrho}{\mathrm{v}}.$$

The term $\mathtt{M_s}$ compares the deformation time scale S_0^{-1} to the acoustic propagation time scale ℓ/a_0, $\mathtt{M_n}$ compares the baroclinic effects time scale N_0^{-1} (due to density stratification and acceleration field [30]) to the acoustic time scale, and $\mathtt{M_a}$ compares the buoyancy force times scale A_0^{-1} to the acoustic time scale. The frequency A_0 is not as usual as S_0 or N_0 in the literature, so we recall its meaning: A_0^{-1} is the time required for a fluid particle of relative density ϵ_ϱ in an acceleration field G_0 to reach the velocity v characteristic of turbulent fluctuations. In other words, A_0 is a measure of the buoyancy force's intensity with respect to turbulence.

Together with these three Mach numbers, we introduced a dimensionless number ξ comparing the evolution time scale of the turbulent field to the time scale of turbulent nonlinear

effects:

$$\xi = \frac{t_0}{\tau}.$$

In particular, evolution and nonlinear time scales are different in the rapid distortion regime.

Finally, the terms related to molecular transport are characterized by the turbulent Reynolds number

$$\mathrm{Re}_t = \frac{\rho_0 \mathrm{v} \ell}{\eta_0}.$$

III. ASYMPTOTICS OF LOW-TURBULENCE MACH NUMBERS

In this section, we perform an asymptotic analysis with respect to the Mach number for a mixture governed by Eq. (13)–(15) subject to fluctuations of its density and polytropic index γ_1. The goal of this analysis is to clarify the conditions under which a pseudocompressible limit can be reached and then to express the properties of pressure and velocity divergence fields in this limit.

First, it is clear that a pseudocompressible limit can exist only if pressure fluctuations equilibrate with their environment on time scales much smaller than all other characteristic times. This means that the pseudocompressible limit can be reached only if

$$\mathtt{M_t} \ll 1, \quad \mathtt{M_s} \ll 1, \quad \mathtt{M_n} \ll 1, \quad \mathtt{M_a} \ll 1. \tag{16}$$

If any one of these conditions is not fulfilled, acoustic effects occur.

Since several small parameters appear, it is necessary to specify their relative order before proceeding to an asymptotic analysis. This issue is actually linked to the existence of two possible regimes for the turbulent flow. These two regimes are defined by the Froude numbers associated with the deformation $\mathcal{F}_u$ and the baroclinic effects $\mathcal{F}_g$, respectively,

$$\mathcal{F}_u = \frac{1}{S_0 \tau} = \frac{\mathtt{M_t}}{\mathtt{M_s}}, \quad \mathcal{F}_g = \frac{1}{N_0 \tau} = \frac{\mathtt{M_t}}{\mathtt{M_n}}.$$

When $\mathcal{F}_u \gtrsim 1$ and $\mathcal{F}_g \gtrsim 1$, i.e., $\mathtt{M_s} \lesssim \mathtt{M_t}$ and $\mathtt{M_n} \lesssim \mathtt{M_t}$, the flow undergoes only weak accelerations or deformations. This is the diffusion-dissipation regime. In contrast, when $\mathcal{F}_u \ll 1$ or $\mathcal{F}_g \ll 1$, i.e., $\mathtt{M_t} \ll \mathtt{M_s}$ or $\mathtt{M_t} \ll \mathtt{M_n}$, the flow undergoes strong accelerations or deformations. The interaction between the mean and the turbulent flows becomes dominant with respect to the interaction of the turbulence with itself (for instance, with respect to straining and sweeping [31]). This is the rapid distortion regime of turbulence.

These definitions lead to two important points. First, there are limitations to the coexistence of the RDT regime and pseudocompressible approximation. Indeed, the conditions $\mathtt{M_s} \ll 1$ and $\mathtt{M_n} \ll 1$ from Eq. (16) imply

$$\mathcal{F}_u \gg \mathtt{M_t}, \quad \mathcal{F}_g \gg \mathtt{M_t}. \tag{17}$$

In order for the pseudocompressibility assumption to remain valid, accelerations and deformations cannot become too strong.

Second, the ordering of Mach numbers depends on the flow regime. Then, the asymptotic developments are different in the RDT regime and in the diffusion-dissipation regime. Both cases should be treated separately.

A. Asymptotics in the diffusion-dissipation regime

The diffusion-dissipation regime is defined from the conditions

$$\mathtt{M_s} \lesssim \mathtt{M_t}, \quad \mathtt{M_n} \lesssim \mathtt{M_t}, \quad \mathtt{M_a} \lesssim \mathtt{M_t}. \tag{18}$$

The relevant time scale in that regime is the turbulent time τ since nonlinear effects are dominant. It leads to set $\xi = 1$ in Eqs. (13)–(15).

Assuming that the turbulent Mach number $\mathtt{M_t}$ is small with respect to 1, the pseudocompressible conditions (16) are fulfilled. The fluctuating quantities $\boldsymbol{U}''$, ρ', p', and γ' are developed as functions of $\mathtt{M_t}$ according to

$$q' = q^{(0)} + \mathtt{M_t} q^{(1)} + \mathtt{M_t^2} q^{(2)} + O\left(\mathtt{M_t^3}\right)$$

for any fluctuating quantity q'. The fluctuating density equation (13) is compatible with these developments under the condition

$$\mathtt{M_n} \lesssim \sqrt{\mathtt{M_a M_t}} \lesssim \mathtt{M_t}. \tag{19}$$

Injecting the developments into Eq. (14) and collecting terms of $O(\mathtt{M_t^{-2}})$ and $O(\mathtt{M_t^{-1}})$ leads to the classical result [2]

$$\frac{\partial p^{(0)}}{\partial x_i} = \frac{\partial p^{(1)}}{\partial x_i} = 0.$$

Thus, the fluctuating pressure follows the usual decomposition $p' = p_c(t) + p_h(t,\boldsymbol{x})$ [2] where $p_c(t) = p^{(0)}(t) + \mathtt{M_t} p^{(1)}(t)$ is a spatially constant pressure of order 0 and $p_h(t,\boldsymbol{x}) = \mathtt{M_t^2}\ p^{(2)}(t,\boldsymbol{x})$ is an hydrodynamical pressure of order 2.

Spatially constant fluctuating pressure with variations of the order of the mean pressure are unlikely to occur in shock tubes, so we exclude that case. A rigorous argument can be provided when a spatial ergodicity hypothesis can be invoked, such as in the case of homogeneous turbulence or shock tube experiments with homogeneity directions. Indeed, when ensemble averaging coincides with spatial averaging, $p_c(t)$ becomes its own mean value $p_c(t) = \overline{p_c(t)}$. Since p_c is the dominant component of a fluctuating pressure with zero mean, one can conclude that $p_c = 0$.

In the following, p_c is consequently assumed to be 0. Then, there is only one fluctuating pressure component left of order $\mathtt{M_t^2}$:

$$p' = M_t^2\ p^{(2)}(t,\boldsymbol{x}). \tag{20}$$

The instantaneous pressure splits into

$$P = \overline{P}(t,\boldsymbol{x}) + M_t^2\ P'^{(2)}(t,\boldsymbol{x}).$$

This decomposition is slightly different from the usual one [2] since the dominant component of the instantaneous pressure can vary in space and have any evolution, including a fully compressible one. Both decompositions coincide only when the mean flow itself obeys a low-Mach-number approximation.

In the next step, the result of Eq. (20) is inserted in Eq. (15). Two cases must be distinguished. In the first one, we assume that density and polytropic index fluctuations are strong:

$$\epsilon_\varrho \sim \epsilon_\gamma \sim 1.$$

This leads, at order 0, to

$$\nabla\cdot\boldsymbol{u}'^{(0)} = \left[\frac{\epsilon_\varrho}{\mathrm{Pr}\,\mathrm{Re}_t}\right]\frac{1}{\overline{\gamma_1}\,\overline{P}}\mathcal{D}'^{(0)} - \left[\frac{\epsilon_\gamma \mathtt{M_s}}{\mathtt{M_t}}\right]\frac{\gamma_1'^{(0)}}{\overline{\gamma_1}}\nabla\cdot\overline{\boldsymbol{U}} - [\epsilon_\gamma]\left(\frac{\gamma_1'^{(0)}}{\overline{\gamma_1}}\nabla\cdot\boldsymbol{u}'^{(0)} - \overline{\frac{\gamma_1'^{(0)}}{\overline{\gamma_1}}\nabla\cdot\boldsymbol{u}'^{(0)}}\right). \quad (21)$$

Then, the velocity divergence depends, at first order, on the molecular transport as well as on the variations of the polytropic index and mean velocity divergence. The first term on the right-hand side of Eq. (21) shows that the volume of a fluid particle is modified by the molecular diffusion of heat and species. The second term of Eq. (21) is related to the volume adjustment of a mass element undergoing compression or dilatation and having a polytropic index different from its environment. The last term comes from the nonlinearity of the coupling between the velocity divergence and polytropic index.

In the second case, density and polytropic index fluctuations are assumed to be weak

$$\epsilon_\varrho \sim \epsilon_\gamma \sim \mathtt{M_t}.$$

This leads, at orders 0 and 1, to

$$\nabla\cdot\boldsymbol{u}'^{(0)} = 0, \quad (22)$$

$$\nabla\cdot\boldsymbol{u}'^{(1)} = -\left[\frac{\mathtt{M_a}}{\epsilon_\varrho}\right]u_j'^{(0)}\frac{1}{\overline{\gamma_1}\,\overline{P}}\frac{\partial\overline{P}}{\partial x_j} - \left[\frac{\epsilon_\gamma\mathtt{M_s}}{\mathtt{M_t^2}}\right]\frac{\gamma_1'^{(0)}}{\overline{\gamma_1}}\nabla\cdot\overline{\boldsymbol{U}} + \left[\frac{\epsilon_\varrho}{\mathtt{M_t}\,\mathrm{Pr}\,\mathrm{Re}_t}\right]\frac{1}{\overline{\gamma_1}\,\overline{P}}\mathcal{D}_p'^{(0)}. \quad (23)$$

The divergence is then of order 1. It depends on molecular transport and polytropic index variations as well as on velocity fluctuations: The first term of Eq. (23) expresses the volume adjustment of a mass element moving along a pressure gradient.

B. Asymptotics in the rapid distortion regime

We now look at the rapid distortion regime of turbulence, which is defined by

$$\mathtt{M_s} \gg \mathtt{M_t} \quad \text{or} \quad \mathtt{M_n} \gg \mathtt{M_t}. \quad (24)$$

First, we will consider the case $\mathtt{M_s} \lesssim \mathtt{M_n}$. In that regime, the relevant time scale is that of baroclinic effects $t_0 = N_0^{-1}$. This leads to $\xi = \mathcal{F}_g = \mathtt{M_t}/\mathtt{M_n}$ in Eqs. (13)–(15).

Conditions (24) imply that $\mathtt{M_t}$ is no longer the relevant parameter to perform an asymptotic development. Instead, fluctuating variables are expanded according to the stratification Mach number $\mathtt{M_n}$:

$$q' = q^{(0)} + \mathtt{M_n}q^{(1)} + \mathtt{M_n^2}q^{(2)} + \cdots.$$

The fluctuating density equation (13) requires a compatibility condition for this expansion to be possible:

$$\mathtt{M_a} \sim \mathtt{M_n}. \quad (25)$$

Conditions (24) imply that $\mathtt{M_t}$ is at least of order 2. Denoting by $n \geqslant 2$ the order of $\mathtt{M_t}$, the fluctuating velocity (14) leads to

$$\frac{\partial p^{(0)}}{\partial x_i} = \frac{\partial p^{(1)}}{\partial x_i} = \frac{\partial p^{(2)}}{\partial x_i} = \cdots = \frac{\partial p^{(n)}}{\partial x_i} = 0$$

and as in the preceding section

$$p^{(0)} = p^{(1)} = p^{(2)} = \cdots = p^{(n)} = 0.$$

Thus, we finally obtain

$$p' = \mathtt{M_n}\mathtt{M_t}\ p^{(n+1)}(t,\boldsymbol{x}). \quad (26)$$

Hence the order of the fluctuating pressure in the RDT regime is different from the one in the diffusion-dissipation regime (20). In particular, it satisfies $p' \gg \mathtt{M_t^2}$.

Inserting Eq. (26) into Eq. (15) leads to an algebraic expression for the velocity divergence. Three cases can be distinguished.

In the first case, density and polytropic index fluctuations are large $\epsilon_\varrho \sim \epsilon_\gamma \sim 1$. Then, at order 0,

$$\frac{\mathtt{M_t}}{\mathtt{M_n}}\nabla\cdot\boldsymbol{u}'\Big|^{(0)} = -\left[\frac{\epsilon_\gamma\mathtt{M_s}}{\mathtt{M_n}}\right]\frac{\gamma_1'^{(0)}}{\overline{\gamma_1}}\nabla\cdot\overline{\boldsymbol{U}} - \left[\epsilon_\gamma\frac{\mathtt{M_t}}{\mathtt{M_n}}\right]\left(\frac{\gamma_1'^{(0)}}{\overline{\gamma_1}}\nabla\cdot\boldsymbol{u}'\Big|^{(0)} - \overline{\frac{\gamma_1'^{(0)}}{\overline{\gamma_1}}\nabla\cdot\boldsymbol{u}'\Big|^{(0)}}\right). \quad (27)$$

The main contribution to the velocity divergence comes in that case from polytropic index fluctuations.

In the second case, density fluctuations are large but not the polytropic index ones $\epsilon_\varrho \sim 1$ and $\epsilon_\gamma \sim \mathtt{M_t}$. Then, at orders 0 and 1,

$$\nabla\cdot\boldsymbol{u}'^{(0)} = \left[\frac{\epsilon_\varrho}{\mathrm{Pr}\mathrm{Re}_t}\right]\frac{1}{\overline{\gamma_1}\,\overline{P}}\mathcal{D}'^{(0)}, \quad (28)$$

$$\nabla\cdot\boldsymbol{u}'^{(1)} = -\left[\frac{\mathtt{M_s}\epsilon_\gamma}{\mathtt{M_n}\mathtt{M_t}}\right]\frac{\gamma_1'^{(0)}}{\overline{\gamma_1}}\nabla\cdot\overline{\boldsymbol{U}} + \left[\frac{\epsilon_\varrho}{\mathrm{Pr}\,\mathrm{Re}_t}\right]\frac{1}{\overline{\gamma_1}\,\overline{P}}\mathcal{D}_p'^{(1)}. \quad (29)$$

These results show that even in the RDT regime the effects of molecular diffusion on the velocity divergence cannot be neglected if density fluctuations are large. This may appear to be in contradiction with the RDT limit concept; however, this is not the case. The main action of the velocity divergence occurs in the density fluctuation equation (13), where $\nabla\cdot\boldsymbol{u}'$ is one order smaller than the other terms depending on mean gradients (if $\epsilon_\varrho \sim 1$) and therefore can be neglected.

The last case corresponds to weak fluctuations of density and polytropic indices $\epsilon_\varrho \sim \mathtt{M_t}$ and $\epsilon_\gamma \sim \mathtt{M_t}$. Then, at orders 0 and 1,

$$\nabla\cdot\boldsymbol{u}'^{(0)} = 0, \quad (30)$$

$$\nabla\cdot\boldsymbol{u}'^{(1)} = -\left[\frac{\mathtt{M_a}\mathtt{M_t}}{\mathtt{M_n}\epsilon_\varrho}\right]u_j'^{(0)}\frac{1}{\overline{\gamma_1}\,\overline{P}}\frac{\partial\overline{P}}{\partial x_j} - \left[\frac{\mathtt{M_s}\epsilon_\gamma}{\mathtt{M_n}\mathtt{M_t}}\right]\frac{\gamma_1'^{(0)}}{\overline{\gamma_1}}\nabla\cdot\overline{\boldsymbol{U}}. \quad (31)$$

Under these hypotheses, the divergence of the fluctuating velocity is determined uniquely by terms depending on mean gradients. In contrast to the preceding case, its contribution to the density fluctuations evolution is this time non-negligible.

Finally, we mention briefly the case $\mathtt{M_n} \lesssim \mathtt{M_s}$. The expansion then uses $\mathtt{M_s}$ as a parameter. The pressure becomes of order $\mathtt{M_s}\mathtt{M_t}$. The velocity divergence can be approximated with a formula identical to that obtained in the case $\mathtt{M_s} \lesssim \mathtt{M_n}$.

C. Synthesis

The asymptotic analysis of the pseudocompressible limit is different depending on the regime considered: RDT or diffusion dissipation. However, common characteristics can be found. Indeed, even if the validity conditions are not identical [Eqs. (19) and (25)], they mainly involve the conditions (16). Note that in the diffusion-dissipation regime, a small value of turbulent Mach number $\mathtt{M_t}$ is sufficient in order for conditions (16) to be fulfilled, whereas it is not the case in the RDT regime.

Then, even if the orders of the fluctuating pressure are not the same in both regimes, the following relation is always met in the pseudocompressible limit:

$$\frac{p'}{P_0} \ll \mathtt{M_t}. \tag{32}$$

Finally, in both regimes the fluctuating velocity divergence can be approximated by

$$\begin{aligned}\boldsymbol{\nabla}\cdot\boldsymbol{u}' = &-u_j'\frac{1}{\overline{\gamma_1}\,\overline{P}}\frac{\partial\overline{P}}{\partial x_j} - \frac{\gamma_1'}{\overline{\gamma_1}}\boldsymbol{\nabla}\cdot\overline{\boldsymbol{U}} + \frac{1}{\overline{\gamma_1}\,\overline{P}}\mathcal{D}_p' \\ &- \left(\frac{\gamma_1'}{\overline{\gamma_1}}\boldsymbol{\nabla}\cdot\boldsymbol{u}' - \overline{\frac{\gamma_1'}{\overline{\gamma_1}}\boldsymbol{\nabla}\cdot\boldsymbol{u}'}\right).\end{aligned} \tag{33}$$

This expression is also valid when both density and polytropic index fluctuations are of main order. The last term on the right-hand side involves the velocity divergence so that Eq. (33) is an implicit relation. However, when polytropic index fluctuations become weak ($\epsilon_\gamma \sim \mathtt{M_t}$) this nonlinear term becomes negligible with respect to the other contributions and the relation becomes explicit.

D. Validity for shock tube experiments

An important question is to know whether the validity conditions of the pseudocompressible approximation [see Eq. (16)] can be met in typical shock tube experiments such as the ones of Poggi *et al.* [32]. No precise and definitive answer can be given, as the variety of phenomena encountered in shock tubes is very wide. Nonetheless, some general comments can be made.

Indeed, we recall that in typical shock tube experiments, turbulent mixing zones are created by some interfacial instability and are subsequently submitted to interactions with shocks as well as compression and rarefaction waves. The latter can induce RDT phases. In between interactions, turbulence is left to decay and undergoes a regime of diffusion-dissipation.

For diffusion-dissipation phases, the validity conditions (16) are fulfilled as soon as the turbulent Mach number $\mathtt{M_t}$ is weak. In practice, it is generally difficult to get even moderate turbulent Mach numbers in shock tube experiments, so the pseudocompressible approximation is indeed relevant for diffusion-dissipation phases.

In contrast, the pseudocompressible approximation becomes meaningless when a shock wave interacts with a turbulent mixing zone. The interaction creates an acoustic field that is initially strongly correlated to the nonacoustic field. Later on, acoustic and nonacoustic fields become uncorrelated anew. Indeed, the acoustic waves do not travel at the material speed, so they are evacuated out of the mixing zones. The acoustic-nonacoustic decorrelation time scale is on the order of the turbulent time scale. As a result, the pseudocompressible approximation cannot be used for about one turbulent characteristic time after shock passage.

As for RDT phases, it is not possible to get a general result *a priori*. The pseudocompressible validity depends on the strain, the stratification, and the acceleration of the mean flow, which depend on the experimental conditions. It is only possible to estimate it for given experimental configurations.

The preceding discussion concerns only the turbulent stage of shock tube experiments. It is indeed the main focus of this work. A few words can nonetheless be added on the early linear and nonlinear phases of the Richtmyer-Meshkov instability happening before the turbulent stage [33]. First of all, let us emphasize that the asymptotic analysis detailed in this study is directly derived from the compressible Navier-Stokes equations. These equations can describe the linear, nonlinear, and turbulent phases of the Richtmyer-Meshkov instability. As a consequence, the asymptotic analysis detailed in this study is valid for all of these phases. Thus, the pseudocompressible approximation will apply to the linear and nonlinear phases of the Richtmyer-Meshkov instability provided conditions (16) are met. During these early phases, mean gradient effects usually become negligible after the shock has crossed the initial interface. Then, we can conclude that the pseudocompressible approximation will be relevant to the early phases of the Richtmyer-Meshkov instability provided the initial postshock turbulent Mach number is small. This is almost always the case in shock tube experiments.

We now focus again on the turbulent regime of shock tube experiments. The considerations we made on this turbulent regime can be illustrated with the experiments of Poggi *et al.* [32]. The experimental setup is a shock tube filled with SF6 in one part of the tube and air in the other part. A turbulent mixing zone is produced by a shock wave of Mach 1.45 (in the SF6) hitting the initial interface between SF6 and air. Other interactions with shock or rarefaction waves occur later due to wall reflections.

This experiment has been simulated with the Grégoire-Souffland-Gauthier (GSG) second-order turbulence model [23]. Comparisons shown in Ref. [23] are globally satisfying. We consequently expect the results obtained with the GSG model, and described hereafter, to yield, at least, correct orders of magnitude. This is sufficient for analyzing the validity conditions (16).

Figures 1(a) and 1(b) respectively show the evolution of the Mach numbers $\mathtt{M_t}$, $\mathtt{M_s}$, $\mathtt{M_n}$, and $\mathtt{M_a}$ and the Froude numbers $\mathcal{F}_u$ and $\mathcal{F}_g$ in the shock tube experiment of Poggi *et al.* [32]. These dimensionless numbers are calculated with the GSG model in the center of the mixing zone produced by the shock crossing the SF6-air interface. To interpret Fig. 1 we use the value 0.3 as a threshold for the condition *small relative to 1*. This choice is frequent in the literature, at least for Mach numbers [2,4].

In Fig. 1, one first observes a phase of initialization of turbulence corresponding to the interaction of the shock wave with the interface at $t = 0$ ms (the choice of time origin in Ref. [32]). Then, it is seen that the mixing zone evolves most of the time in a diffusion-dissipation regime. Conditions (16) are then fulfilled since the turbulent Mach number is small.

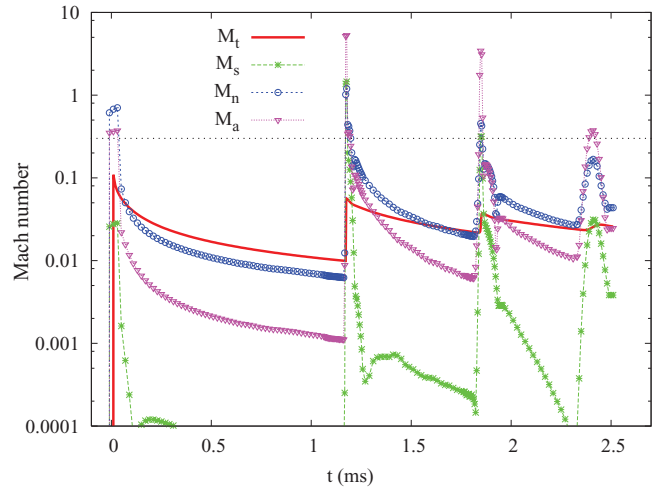

FIG. 1. (Color online) Simulation of the shock tube experiment of Poggi *et al.* [32] with the GSG second-order model [23]: (a) Mach numbers and (b) Froude numbers in the middle of the mixing zone with respect to time.

Furthermore, one can notice a RDT phase ($\mathcal{F} < 0.3$) beginning at $t \approx 2.3$ ms. This RDT regime is due to stratification and not to mean flow straining. During this RDT regime, conditions (16) are fulfilled, except the condition $\mathtt{Ma} \ll 1$. Indeed a value $\mathtt{Ma} \sim 0.4$–0.5 is reached. It can be expected that acoustic effects occur during this phase, but remain moderate. Finally, reshocks are observed at $t \approx 1.2$ and 1.8 ms, indicating the times when the pseudocompressible approximation definitely cannot be applied.

IV. CONSEQUENCES OF THE PSEUDOCOMPRESSIBLE APPROXIMATION ON STATISTICAL MODELS

The purpose of this section is to show how the asymptotic results derived so far can help improve second-order one-point models used for predicting shock tube experiments such as those of Grégoire *et al.* [23], Banerjee *et al.* [24], Besnard *et al.* [25], or Andronov *et al.* [26]. A detailed review on one-point models for variable density flows, including second-order models, is also presented by Chassaing *et al.* [34]. We hereafter emphasize two aspects of these models that are impacted by the pseudocompressible approximation. The first one concerns the evolution of the density flux and variance and the second one concerns the transport of enthalpy.

A. Density flux and variance evolutions

All the aforementioned models aim at predicting the evolutions of the joint correlations of velocity and density or of a subset of equivalent quantities. For instance, the model of Grégoire *et al.* [23] is derived by closing evolution equations for the Reynolds stresses $\widetilde{u_i'' u_j''}$, density variance $\overline{\rho'^2}$, and density flux $\overline{u_i''} = -\overline{\rho' u_i'}/\overline{\rho}$.

The evolutions of the latter two quantities are intimately linked to the fluctuating velocity divergence. More precisely, up to second-order correlations and viscous effects, the evolutions of $\overline{\rho'^2}$ and $\overline{u_i''}$ are given by

$$\frac{\partial \overline{\rho'^2}}{\partial t} + \widetilde{U}_j \frac{\partial \overline{\rho'^2}}{\partial x_j} = -2\overline{\rho}\,\overline{\rho' \nabla \cdot \boldsymbol{u}'} - 2\overline{\rho'^2} \nabla \cdot \widetilde{\boldsymbol{U}} + 2\overline{\rho} \overline{u_j''} \frac{\partial \overline{\rho}}{\partial x_j} + (\text{third-order terms}), \tag{34}$$

$$\frac{\partial \overline{u_i''}}{\partial t} + \widetilde{U}_j \frac{\partial \overline{u_i''}}{\partial x_j} = \overline{u_i' \nabla \cdot \boldsymbol{u}'} - \overline{u_j''} \frac{\partial \widetilde{U}_i}{\partial x_j} - \frac{\overline{\rho'^2}}{\overline{\rho}^2} \frac{1}{\overline{\rho}} \frac{\partial \overline{P}}{\partial x_i} + \widetilde{u_i'' u_j''} \frac{1}{\overline{\rho}} \frac{\partial \overline{\rho}}{\partial x_j} + \overline{\frac{\rho'}{\rho} \frac{1}{\overline{\rho}} \frac{\partial P'}{\partial x_i}} + \overline{\frac{\rho'}{\rho} \frac{\partial \sigma_{ij}'}{\partial x_j}} + (\text{third-order terms} + \text{viscous terms}). \tag{35}$$

One can see that the only second-order unclosed term in the density variance evolution is the correlation $\overline{\rho' \nabla \cdot \boldsymbol{u}'}$ and that the correlation $\overline{u_i' \nabla \cdot \boldsymbol{u}'}$ appears as a source term in the equation for the turbulent density flux.

These two quantities can be straightforwardly modeled by using the pseudocompressible expression of the velocity divergence (33). Neglecting all third-order correlations, we obtain

$$\overline{\frac{\rho'}{\rho} \nabla \cdot \boldsymbol{u}'} = \overline{u_j''} \frac{1}{\overline{\gamma_1} \overline{P}} \frac{\partial \overline{P}}{\partial x_j} + \frac{\overline{\gamma_1''}}{\overline{\gamma_1}} \nabla \cdot \overline{\boldsymbol{U}} - \frac{1}{\overline{\gamma_1} \overline{P}} \overline{\mathcal{D}_p''}, \tag{36}$$

$$\overline{u_i' \nabla \cdot \boldsymbol{u}'} = -\widetilde{u_i'' u_j''} \frac{1}{\overline{\gamma_1} \overline{P}} \frac{\partial \overline{P}}{\partial x_j} - \overline{\frac{\gamma_1'}{\gamma_1} u_i'} \nabla \cdot \overline{\boldsymbol{U}} + \frac{1}{\overline{\gamma_1} \overline{P}} \overline{u_i' \mathcal{D}_p'}. \tag{37}$$

The main interest in these relationships is to make explicit the dependence of the two unknown correlations $\overline{\rho' \nabla \cdot \boldsymbol{u}'}$ and $\overline{u_i' \nabla \cdot \boldsymbol{u}'}$ on the mean pressure and velocity gradients. Equations (36) and (37) also introduce a dependence on the equation of state through the fluctuations of the polytropic index γ_1, whose correlations with the density and velocity can be easily expressed by a proper linearization. Finally, molecular mixing is also involved in these expressions through the correlations of $\mathcal{D}_p'$ with density and velocity.

In most of the mentioned second-order models [23–25], the only terms that are implicitly accounted for when closing $\overline{\rho' \nabla \cdot \boldsymbol{u}'}$ and $\overline{u_i' \nabla \cdot \boldsymbol{u}'}$ are the molecular mixing terms. They are generally closed in the form of dissipation terms for the density variance and density flux. For turbulent flows close to equilibrium, this is certainly a sufficient approximation. However, in the context of shock tube experiments, the role

played by the mean pressure and velocity gradients is crucial and should not be neglected. This assertion can be checked by considering the interaction of a homogeneous turbulent field with an isentropic mean flow, such as a rarefaction wave. In that case, the pressure gradient terms in Eqs. (36) and (37) cancel out with the production of $\overline{\rho'^2}$ and $\overline{u_i''}$ by mean density gradients. Furthermore, the mean velocity gradient term in Eq. (36) becomes the only source of density variance. Thus, for the particular case detailed here, the evolutions of $\overline{\rho'^2}$ and $\overline{u_i''}$ would not be consistent if the mean pressure and velocity gradient terms were neglected in Eqs. (36) and (37).

B. Turbulent enthalpy transport

Another key aspect of the turbulent models used in shock tube experiments lies in the closure of the turbulent transport of enthalpy (or energy, depending on the precise model formulation). Most often the enthalpy flux $\widetilde{u_i''h''}$ is closed due to a gradient diffusion assumption. In contrast, the density flux follows an evolution equation, which, in some circumstances, can yield countergradient transport. However, the enthalpy and density flux are intimately linked. For instance, for an isobaric isotemperature mixture of perfect gases, they are directly proportional to one another.

The pseudocompressible approximation allows one to express the enthalpy flux in a more coherent way. Indeed, the asymptotic analysis of Sec. III gives a rationale for neglecting pressure fluctuations in the equation of state of the flow. Then, the enthalpy fluctuation can be linearized and expressed as a function of the density and concentration fluctuations. As a result, one obtains the following expression for the enthalpy flux, after neglecting third-order correlations:

$$\widetilde{u_i''h''} = \left[\frac{\overline{\gamma}_1}{\overline{\gamma}_3 - 1}\frac{\overline{P}}{\overline{\rho}}\right]\overline{u_i''} - \left[\frac{\overline{\gamma}_3}{\overline{\gamma}_3 - 1}\frac{\overline{P_\alpha}}{\overline{\rho}} - \overline{h_\alpha}\right]\widetilde{u_i''Y_\alpha''}. \quad (38)$$

The connection between the enthalpy and density fluxes is thus made explicit, as well as its dependence on the concentration fluxes. Such an expression can, in principle, be used in the models proposed in Refs. [23–26].

V. DIRECT NUMERICAL SIMULATION OF THE INTERACTION OF A RAREFACTION WAVE WITH A MIXING ZONE

In order to check the hypotheses and consequences of the pseudocompressible approximation, we perform three-dimensional direct numerical simulations (DNSs) with the TRICLADE code. Different numerical methods are available in this massively parallel code. Here we use a conservative finite-difference scheme based on the work of Daru and Tenaud [35]. The same method was employed in our previous work [36,37] involving simulations of turbulent mixture interactions with shock waves.

The TRICLADE code solves Eqs. (2)–(4) in conservative form. The equation of state (5) is obtained for a mixture of perfect gases by assuming that the mixture is isothermal and obeys Dalton's law of partial pressures. Denoting for each perfect gas the adiabatic exponent by γ_α and the constant volume specific heat by $c_{v\alpha}$, the equation of state (5) can be written as

$$P = (\gamma - 1)\rho e \quad \text{for } \gamma - 1 = \frac{\sum_{\alpha=1}^{N_s}(\gamma_\alpha - 1)c_{v\alpha}Y_\alpha}{\sum_{\alpha=1}^{N_s} c_{v\alpha}Y_\alpha}. \quad (39)$$

In the present case, only a binary mixture is considered, which means $N_s = 2$. The molecular transport fluxes (10)–(12) are simplified by using Stokes assumption that $\kappa = 0$ and assuming a single viscosity and conductivity coefficient for both gases; since $N_s = 2$, there is only a single interspecific diffusion coefficient.

A. Flow configuration

1. Overview of the simulation

The purpose of the simulation is to study the interaction of a rarefaction wave with a turbulent mixing zone in conditions close to the RDT regime. To this end, the simulation unfolds in two steps. During the first step, a turbulent mixing zone is produced by a Richtmyer-Meshkov instability. Then, during the second step, a rarefaction wave is sent to this mixing zone.

The configuration consists in an idealized planar shock tube containing air and argon initially separated by a corrugated interface. In the first step, a shock wave of moderate Mach number (1.25) coming from the air side interacts with the initially corrugated interface. As a result of the interaction, a shock wave is transmitted into argon, another one is reflected into air, and vorticity is deposited on the interface, yielding a growth of the interface corrugation amplitude. This instability mechanism is of course known as Richtmyer-Meshkov instability. The instability leads to the interpenetration of both media and eventually a mixing zone appears between them.

When the transmitted and reflected shock waves are far enough, we proceed with the second step. We extract the mixing zone and insert a rarefaction wave in the part of the domain containing air. That procedure is detailed as follows. Immediately after interaction, acoustic waves reverberate between the interface and the outgoing shock fronts, but their amplitudes quickly decrease as the shock fronts go farther. As a result, the flow between the mixing zone and the shock waves eventually becomes uniform. At the time of extraction, we choose two abscissas x^- and x^+ enclosing the mixing zone but inside both uniformly shocked fluid zones. Then we erase the shock waves by replacing all state variables for $x > x^+$ ($x < x^-$) by the average value of corresponding quantity at x^+ (x^-). The final step consists in introducing a one-dimensional rarefaction by analytically computing its profiles in a single gas, the air, for an upstream state given by the state at x^-. All quantities at the abscissa downstream from the chosen rarefaction head are then replaced by the analytical ones. Using Galilean invariance, a longitudinal translation velocity is also added so that the mixing zone remains in the central part of the computational domain, with the finest mesh, for the largest time.

The first part of the simulation is similar to other simulations such as that of Thornber *et al.* [38]. As explained, it is not the main focus of this simulation. It should only be considered as a preliminary step needed to study the subsequent interaction of the rarefaction wave and mixing zone.

2. Initial conditions

(a) Preliminary step. Before the shock interaction, both air and argon are initially at rest at standard conditions of pressure 10^5 Pa and temperature 290 K. The polytropic indices of air and argon are 1.4 and 1.66, respectively. Their constant volume heat capacities are set to 720 and 310 $\mathrm{J\,kg^{-1}\,K^{-1}}$, respectively. The dynamic viscosity is $\mu = 5 \times 10^{-5}\ \mathrm{kg\,m^{-1}\,s^{-1}}$ and the Schmidt and Prandtl numbers are on the order of 1.

The interface corrugation has a broadband spectrum with a maximum around wavelength $\lambda_{\max} = 1.4 \times 10^{-3}$ m and a large rms amplitude around 3.7×10^{-4} m. The shock Mach number is $M_s = 1.25$, thus the velocity jump of the mean interface due to shock interaction is $\Delta U \approx 110\ \ \mathrm{m\,s^{-1}}$. It is customary to define a Reynolds number based on ΔU as $\rho\, A_t\, \Delta U\, \lambda_{\max}/\mu$ with a value $\sim$1000 in our simulation. Note that this Reynolds number has no physical meaning, just a dimensioning interest. In contrast to the wavelength $\lambda_{\max}$, the jump velocity ΔU indeed characterizes the mean flow, but not the perturbed flow. For a single-mode initial spectrum at wave number κ_0 with amplitude a_0, a meaningful Reynolds number should rather be constructed based on the perturbation velocity $a_0 \kappa_0 A_t \Delta U$.

(b) Main step. At time $t_{\mathrm{ex}} = 3.4\lambda_{\max}/\Delta U$, the transmitted and reflected shock waves are far enough from the mixing zone to proceed with the main step of the simulation, i.e., the extraction of the mixing zone and the injection of the rarefaction wave.

At that time, the mixing zone has the following characteristics. First, its Atwood number is $A_t = \frac{\rho_{\mathrm{Ar}} - \rho_{\mathrm{air}}}{\rho_{\mathrm{Ar}} + \rho_{\mathrm{air}}} \approx 0.13$. In addition, in the middle of the mixing zone, the turbulent length scale is $\ell_0 = \widetilde{k}^{3/2}/\widetilde{\varepsilon} \approx 0.3\lambda_{\max}$ and the turbulent velocity is $\mathrm{v}_0 = \sqrt{2\widetilde{k}/3} \approx 0.03\Delta U$, where $\widetilde{k} = ||\widetilde{\boldsymbol{u}''}||^2/2$ is the average specific kinetic energy and $\widetilde{\varepsilon}$ is the average viscous dissipation. The length of the mixing zone is $L_{\mathrm{MZ}} \approx 4.85\ell_0$. Finally, the turbulent Reynolds number $\mathrm{Re}_t = \widetilde{k}^2/\nu\widetilde{\varepsilon}$ is slightly larger than 80 in the middle of the mixing zone. This value is weak compared to the Reynolds number in the experiment of Poggi *et al.* [32], which is of order 10^3 after the first interaction and of order 10^4 after the first reshock. While more realistic values of Re_t would be of interest, a low Reynolds number does not in any way impede the assessment of the pseudocompressible approximation. More important are the values of the four Mach numbers $\mathtt{M_t}$, $\mathtt{M_s}$, $\mathtt{M_n}$, and $\mathtt{M_a}$. Those are indeed found to be on the order of the ones observed in shock tube experiments, as will be detailed in the following sections (see Fig. 3).

The two abscissas enclosing the mixing zone and defining the zone of extraction are set equal to $x^- \approx -10\ell_0$ and $x^+ \approx 10\ell_0$, with $x = 0$ corresponding approximately to the center of the mixing zone at that time. The injected rarefaction wave has a width of $20\ell_0$, with its head placed at $x^H = -7\ell_0$. The rarefaction wave, coming from the air side, has a compression ratio (downstream air density divided by upstream air density) equal to 0.4.

3. Numerical considerations

(a) Boundary conditions and mesh construction. The simulation is three dimensional with doubly periodic conditions in the homogeneous directions. A Cartesian structured mesh is used. The cross section is square with size $13.1\ell_0 \times 13.1\ell_0$ and is meshed with 400×400 cells. The longitudinal direction is divided into three zones. The mixing zone evolves in a central part of the computational domain where the cells are cubic. In that part of length $19.65\ell_0$, there are 600 cells in the longitudinal direction. On both sides of that central part, domains of 240 cells with geometric progression of cell sizes span over $100\ell_0$ so that the boundaries can be considered as infinitely far from the mixing zone. In practice, these boundaries are treated with zeroth-order extrapolation and have no effect on the core region during the time interval of the simulation.

Note that the same mesh is used for the two steps of the computation: No interpolation is needed when going from the preliminary to the main step. The mixing zone content is completely unaffected by the process. Since the Reynolds number is quite weak and high-order numerical schemes are used, every scale involved in the problem is well resolved, thus allowing one to compute precisely all the terms treated or neglected in the pseudocompressible approximation.

(b) Postprocessing. As mentioned previously, the problem is statistically one dimensional and the average operator is defined as the plane average over cross section. Numerically, let $i \in [1, N_\parallel]$ be the mesh index in the longitudinal direction (spanning over $N_\parallel$ cells) and $j,k \in [1, N_\perp]$ be the mesh indices in the homogeneous directions (spanning over $N_\perp$ cells). The instantaneous local averages are obtained as

$$\overline{Q}_i = \frac{\sum_{k=1}^{N_\perp} \sum_{j=1}^{N_\perp} Q_{ijk}}{N_\perp^2},$$

which defines the Reynolds average from which the Favre average and Reynolds and Favre fluctuations are obtained according to the relations recalled in Sec. II B.

From the local values $\overline{Q}_i$, we also define an instantaneous value in the middle of the mixing zone $\overline{Q}_{\mathrm{MZ}}$ intended to be representative of the abscissa where the mass fraction is one-half, but also to behave smoothly in order to get clean temporal evolutions. It is defined in the following way:

$$\overline{Q}_{\mathrm{MZ}} = \frac{\sum_{i=1}^{N_\parallel} \overline{Q}_i \exp\left[-\left(\frac{\tilde{Y}-1/2}{\delta Y}\right)^2\right]}{\sum_{i=1}^{N_\parallel} \exp\left[-\left(\frac{\tilde{Y}-1/2}{\delta Y}\right)^2\right]}.$$

The coefficient δY is chosen to be 2×10^{-2}. Since there are only two gases, there is no ambiguity about the mass fraction choice.

(c) Reference scales, time, and space origins. Numerical results will hereafter be displayed in a nondimensional way. Reference scales are defined as follows. Densities are normalized by $\rho_0 = (\rho_{\mathrm{Ar}} + \rho_{\mathrm{air}})/2$, where ρ_{Ar} and ρ_{air} are the values in pure argon and pure air before interaction with the rarefaction wave. The characteristic length and velocity are chosen as ℓ_0 and v_0. These have been defined in the preceding section as the turbulent length and velocity scale in the middle of the mixing zone at the time of extraction. The mean characteristic time is set as $\tau = \ell_0/\mathrm{v}_0$.

The time origin for displaying results is chosen such that the rarefaction head reaches the middle of the mixing zone at $t = 0$. By middle of the mixing zone we intend the instantaneous location where the averaged mass fraction is equal to one-half.

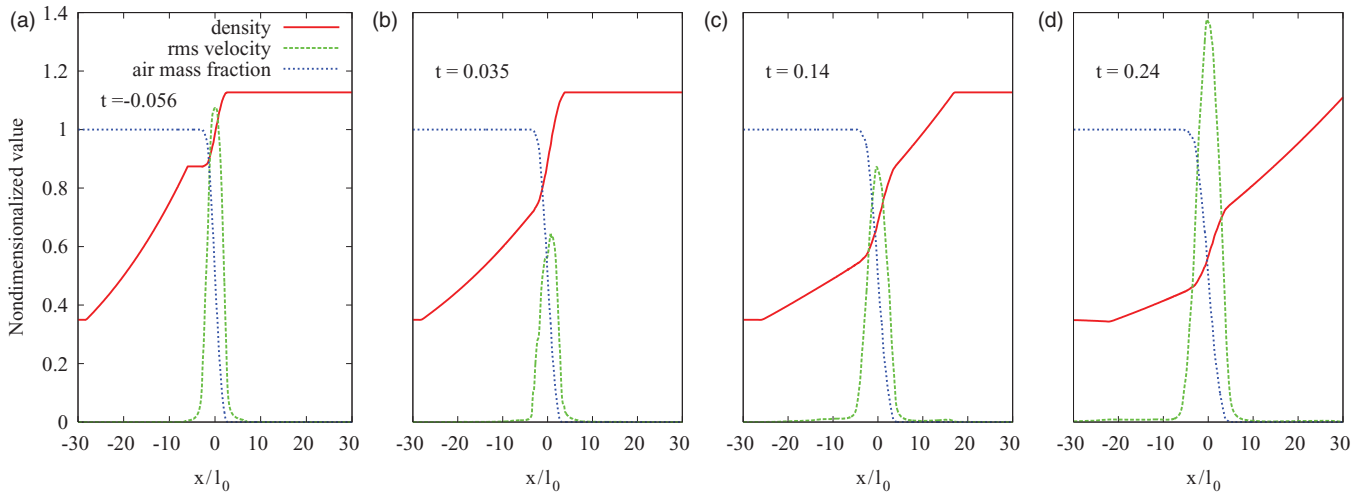

FIG. 2. (Color online) Flow evolution: cross averaged air mass fraction, normalized density $\overline{\rho}/\rho_0$, and rms velocity $\sqrt{2\widetilde{k}/3}/v_0$ with respect to the longitudinal direction x/ℓ_0 before interaction and at different times during interaction.

This location will also serve as spatial origin in the longitudinal direction.

B. Results

We recall that the present work focuses on the rarefaction–mixing-zone interaction. Hence, numerical results are displayed and commented only for the second phase of the calculation.

1. Mean profile evolution

In order to give a general overview on the flow evolution, spatial profiles of three cross-averaged quantities are displayed at different times in Fig. 2 with respect to the longitudinal direction: the air mass fraction, the normalized density $\overline{\rho}/\rho_0$, and the normalized rms velocity $\sqrt{2\widetilde{k}/3}/v_0$.

Figure 2 allows one to see the respective positions of the rarefaction wave and the mixing zone before and during the interaction. The profiles before interaction can be seen in Fig. 2(a). The density profile of this plot allows one to identify the rarefaction incoming from the left and located approximately between $-27\ell_0$ and $-7\ell_0$. The air mass fraction profile shows that the mixing zone spans approximately between $-2.5\ell_0$ and $+2.5\ell_0$. At subsequent times, displayed in Figs. 2(b)–2(d), the mixing zone is entirely enclosed in the rarefaction wave. The concentration field has a trivial evolution due almost completely to the dilatation by the rarefaction, whereas the kinetic energy undergoes much more complex variations due to production and deproduction effects by the mean flow. Note that the interaction creates a stable stratification, which leads to a countergradient situation. This explains why the kinetic energy first decreases before displaying a rebound (see Ref. [30] for more details on oscillating

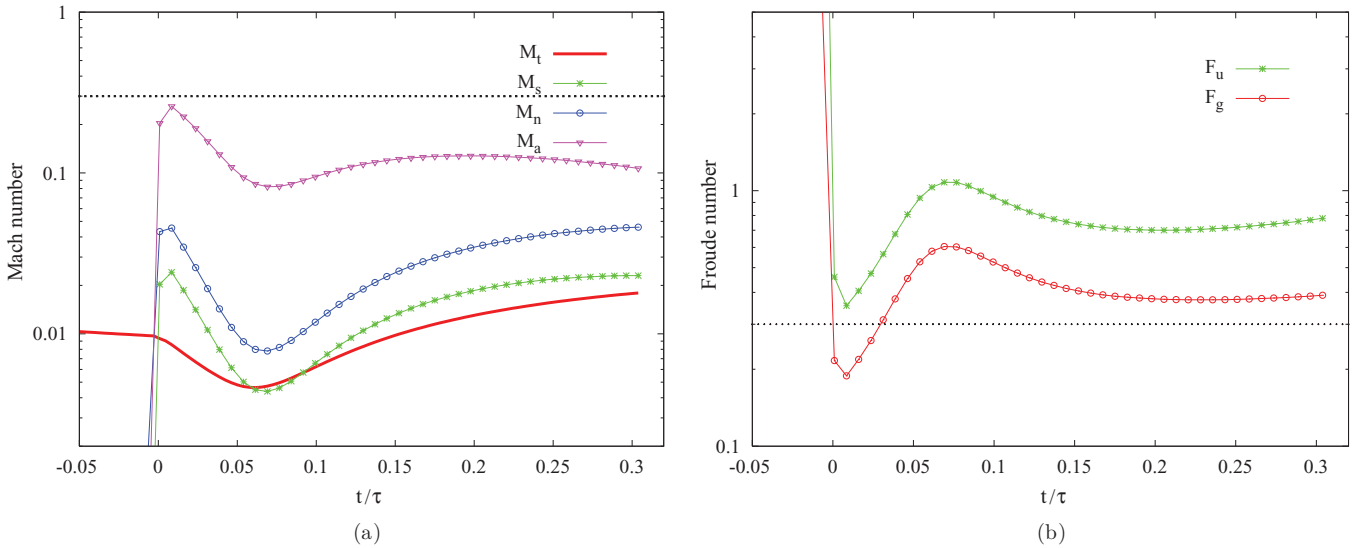

FIG. 3. (Color online) Mach and Froude numbers in the middle of mixing zone with respect to time.

countergradient in stably stratified flows). Such features are characteristic of the predominance of linear production terms.

2. Dimensionless numbers

The characteristic dimensionless numbers relevant to the pseudocompressible asymptotic analysis are the Mach and Froude numbers as well as the ratios of fluctuations to averages of density ϵ_ϱ and polytropic index ϵ_γ. In the simulation, it was observed that ϵ_ϱ and ϵ_γ did not exceed 0.1 and could consequently be considered small compared to one. As for the Mach and Froude numbers, Fig. 3 shows their evolution in the middle of the mixing zone as defined in Sec. V A 3. The evolutions are not monotonic due to the simultaneous action of three effects. First, the mean density gradient has two different contributions, one coming from the stratification of the mixing zone and one imposed by the rarefaction wave. Second, the interaction produces a transmitted rarefaction wave as well as reflected waves leading to a nontrivial evolution. Third, turbulence reacts rapidly to the interaction.

Figure 3(a) shows whether or not the pseudocompressible approximation is valid. Before the interaction $t < 0$, all Mach numbers are weak, pseudocompressible conditions are then fulfilled. At the beginning of the interaction, the Mach numbers are small, except for the buoyancy force Mach number $\mathtt{Ma}$, whose value reaches 0.3. During this period, acoustic effects could play a role. Then, the buoyancy force Mach number decreases and all Mach numbers are weak enough so that the pseudocompressible conditions are fulfilled again.

The Froude number evolution is shown in Fig. 3(b). Before interaction the Froude numbers are large compared to 1; as expected, the regime is of the diffusion-dissipation kind. From $t \approx 0$ to 3×10^{-2}, the Froude number associated with baroclinic effects is lower than 0.3. This value is chosen as a limit value for the RDT regime. The mixing zone evolves in a regime that is not strictly a RDT regime but an intermediate regime where production effects are dominant and diffusion-dissipation effects still play a role. After $t \approx 3 \times 10^{-2}$ the Froude number grows so the regime becomes closer to a diffusion-dissipation one. To sum up, the examination of Fig. 3 lets us distinguish three phases as detailed in Table I.

3. Fluctuating velocity divergence

In this section, we illustrate the validity of the formula (33) for the fluctuating velocity divergence and show that it is useful for turbulent mixing modeling. More precisely, we are interested in the two correlations required for the closure of Reynolds stress models: $\overline{u'\nabla\cdot\boldsymbol{u}'}$, which appears in the equation of the turbulent density flux, and $\overline{\rho'\nabla\cdot\boldsymbol{u}'}/\overline{\rho}$, which appears in the equation of the density variance. Their expressions derived from the pseudocompressible approximation are given by Eqs. (36) and (37). Here these correlations

TABLE I. Phases of the DNS computation.

Time	Regime
[−0.05,0]	pure diffusion-dissipation
[0,0.03]	strong interaction
[0.03,0.15]	weak interaction

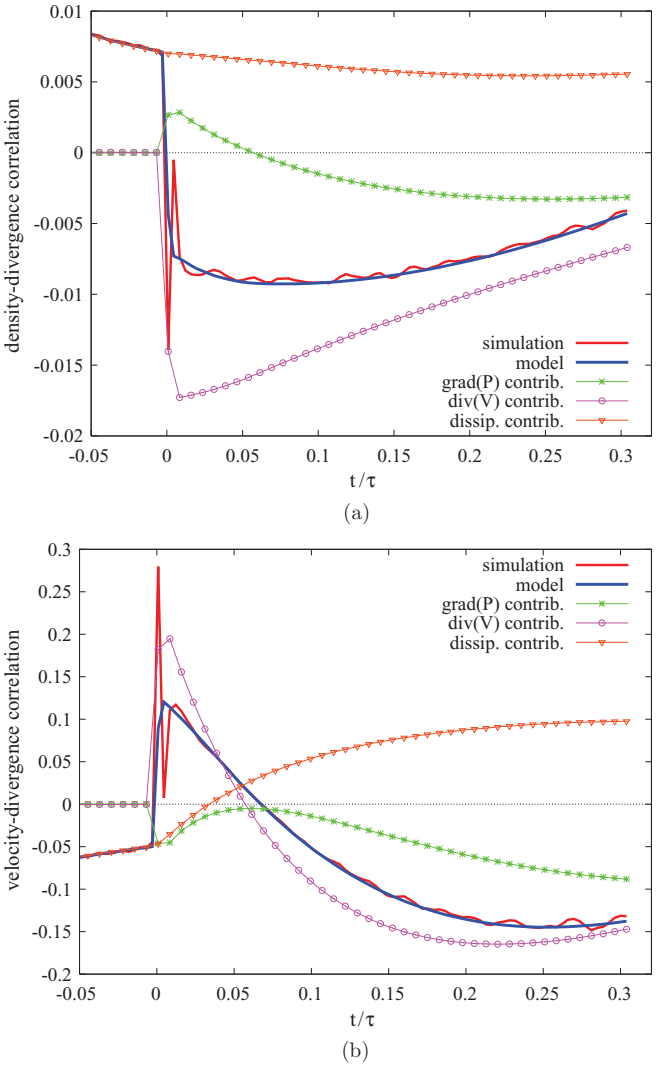

FIG. 4. (Color online) Time evolution of the correlations of the fluctuating velocity divergence with density (a) $\overline{\rho'\nabla\cdot\boldsymbol{u}'}/\overline{\rho}$ and velocity (b) $\overline{u'\nabla\cdot\boldsymbol{u}'}$ in the middle of the mixing zone. Also shown is a comparison between DNS and the pseudocompressible model [Eqs. (36) and (37)].

are made dimensionless with the same characteristic length ℓ and velocity v of the turbulent field as before.

Figures 4(a) and 4(b) show $\overline{u'\nabla\cdot\boldsymbol{u}'}$ and $\overline{\rho'\nabla\cdot\boldsymbol{u}'}/\overline{\rho}$ in the middle of the mixing zone (location of the mass fraction of $\frac{1}{2}$) with respect to time. The lines tagged "simulation" give the computed values of the correlations and the dotted lines tagged "model" show the pseudocompressible model predictions. The contribution of each of the three terms on the right-hand sides of Eqs. (36) and (37) are also given. They are denoted by "grad(P) contrib." for the contribution of the mean pressure gradient terms, "div(V) contrib." for the contribution of the mean velocity divergence terms, and "dissip. contrib." for the contribution of molecular mixing terms.

First, it can be observed in Fig. 4 that all three contributions related to the mean pressure gradient, the mean velocity divergence, and the diffusion-dissipation regime are of the same order of magnitude. Second, the agreement of the low-Mach-number model (given by the sum of the three contributions)

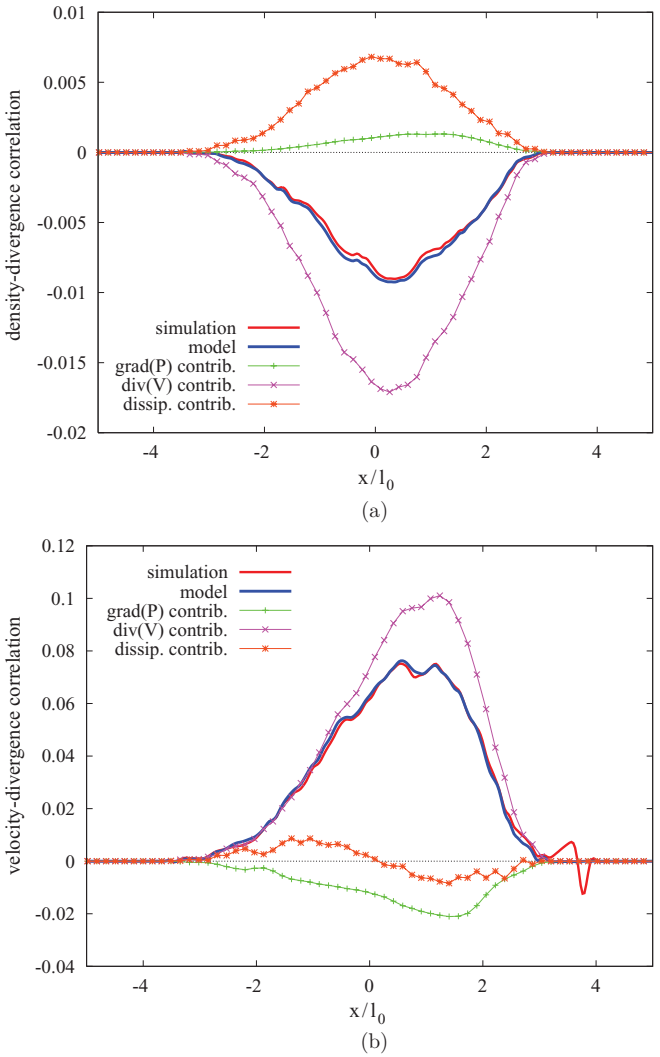

FIG. 5. (Color online) Spatial profiles of the correlations of the fluctuating velocity divergence with density (a) $\overline{\rho' \nabla \cdot \boldsymbol{u}'}/\overline{\rho}$ and velocity (b) $\overline{u' \nabla \cdot \boldsymbol{u}'}$ at dimensionless time $t = 3.5 \times 10^{-2}$ during the interaction with the rarefaction wave. Also shown is a comparison between DNS and the pseudocompressible model [Eqs. (36) and (37)].

with the exact correlation (denoted with "simulation" in Fig. 4) is very good, except at the beginning of the interaction and also for some weak oscillations with time in the exact correlation curve.

These discrepancies can be explained by the fact that the rarefaction head is a weak discontinuity: The primitive fields (density, velocity, and pressure) are continuous, but their longitudinal derivatives jump across the rarefaction head. A closer examination of the fluctuating field at the rarefaction head is possible. As for the mean flow, the fluctuating primitive fields are continuous, but not their derivatives. In the linear limit, jump conditions for the derivatives can be obtained with respect to the fluctuating local values and a single unknown constant originating from the need to specify the whole history of the rarefaction (see the Appendix). For the simulation case, it appears that the fluctuating velocity divergence jumps in response to the interaction with the entropy waves constituting

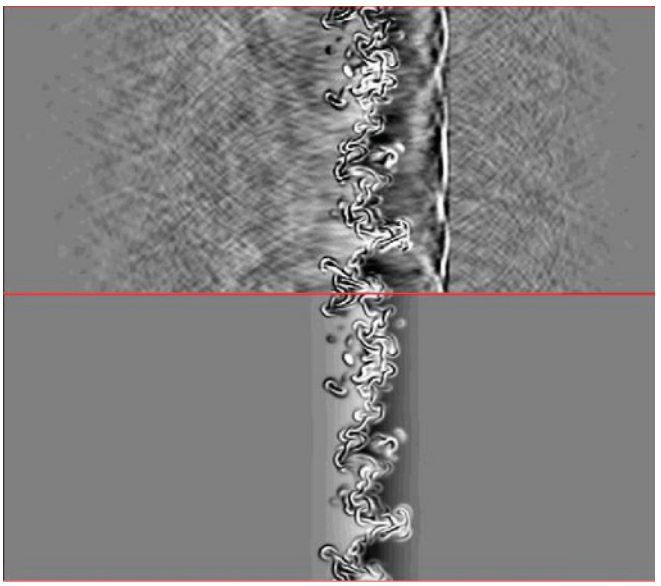

FIG. 6. Fluctuating velocity divergence $\nabla \cdot \boldsymbol{u}'$ cross section as computed in the simulation (top) and filtered according to the low-Mach-number model (33) (bottom) at dimensionless time $t = 3.5 \times 10^{-2}$ during the interaction with the rarefaction wave.

the upstream mixture. This production of velocity divergence at the weak discontinuity produced by the rarefaction head explains the strong but short disagreement with the pseudo-compressible prediction just after $t = 0$.

It is interesting to understand why the pseudocompressible approach fails to reproduce this feature. This can be traced back to the nondimensionalization of the fluctuating field. The latter is made dimensionless with v for velocity and ℓ for the length so that the velocity divergence is scaled by ℓ/v. However, at the rarefaction head the change in mean velocity divergence over an infinitesimally small distance makes the length scale ℓ irrelevant for describing the gradients of the fluctuating field.

Figures 5(a) and 5(b) are the spatial counterparts of Figs. 4(a) and 4(b). Here, the same contributions to correlation are plotted with respect to the dimensionless abscissas at the dimensionless time $t = 3.5 \times 10^{-2}$, which means, according to Table I, in a regime of quite strong interaction but with non-negligible diffusion-dissipation effects. Figure 5 shows very good agreement of the pseudocompressible approximation over the whole turbulent mixing zone. As before, the relative magnitude of the three contributions differs from place to place, but the total always agrees with the exact correlation. The only discrepancy is seen in Fig. 5(b) near abscissa 3.8 and corresponds to the location of the rarefaction head, as explained previously. At that time, the rarefaction tail is on the left of the mixing zone, so the latter is completely inside the rarefaction wave, which is why the mean gradients contributions are dominant.

In order to get a more direct comparison at the same time, we show in Fig. 6 a cross section of the fluctuating velocity divergence directly computed from the simulation and as obtained from the pseudocompressible approximation. It can be inferred that the latter acts as a filter removing all acoustic contributions from the former. Indeed, the acoustic

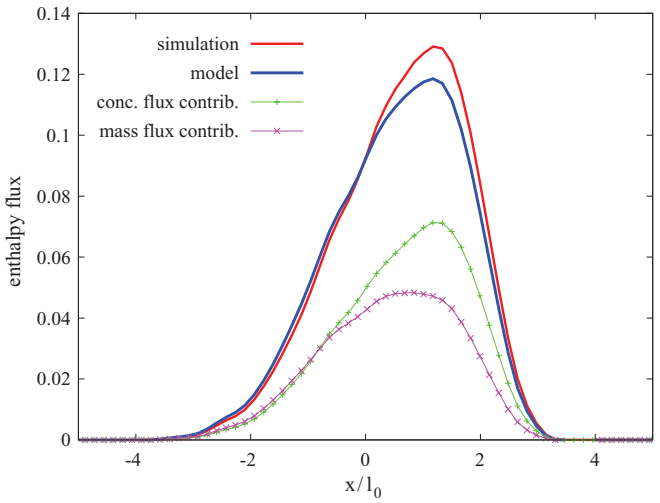

FIG. 7. (Color online) Normalized turbulent enthalpy flux $\widetilde{h''u''}/\tilde{h}$ at dimensionless time $t = 3.5 \times 10^{-2}$ during the interaction with the rarefaction wave. Also shown is a comparison between DNS and the pseudocompressible model [Eq. (38)].

field radiated from the turbulent mixing zone is clearly visible in the direct computation together with the rarefaction head corrugation whereas they are completely removed from the field obtained with the pseudocompressible approximation. This figure also allows one to see that even if both correlations $\overline{u'\nabla\cdot\boldsymbol{u}'}$ and $\overline{\rho'\nabla\cdot\boldsymbol{u}'/\rho}$ are well predicted by the model, the total variance $\overline{(\nabla\cdot\boldsymbol{u}')^2}$ can be quite different from the pseudocompressible one, which retains only the low-Mach-number part of the fluctuating velocity divergence field because the acoustic contribution of the flow is non-negligible in these simulations.

4. *Turbulent enthalpy flux*

Figure 7 shows the profile of the normalized turbulent enthalpy flux $\widetilde{h''u''}/\tilde{h}$ at the same time as in the preceding figures. The values expected from the low-Mach-number model according to Eq. (38) are compared to the simulated ones and contributions from both the mass flux $[\frac{\overline{\gamma}_1}{\overline{\gamma}_3-1}\frac{\overline{P}}{\overline{\rho}}]\overline{u_i''}$ and the concentration flux $-[\frac{\overline{\gamma}_3}{\overline{\gamma}_3-1}\frac{\overline{P_\alpha}}{\overline{\rho}}-\overline{h_\alpha}]\widetilde{u_i''Y_\alpha''}$ are also displayed. Figure 7 shows close agreement between the computed enthalpy flux and the modeled one, except in the middle of the mixing zone where the turbulent intensity is larger, so some triple correlations unaccounted for become non-negligible.

VI. CONCLUSION

In this work we derived a pseudocompressible approximation applicable in the context of shock tube experiments. In particular, it can be applied to turbulent mixing zones with density and polytropic index fluctuations. The mean flow can be time and space varying as well as fully compressible.

The pseudocompressible approximation is obtained via an asymptotic analysis under the hypotheses (16) assuming small values of the turbulent, deformation, stratification, and buoyancy force Mach numbers. The diffusion-dissipation and rapid distortion regimes are treated separately. The main results of the analysis are the order of the fluctuating pressure, which depends on the regime under consideration, and the model (33) for the fluctuating velocity divergence, which is valid for both regimes.

The validity conditions of the pseudocompressible approximation (16) also constitute one of the interests of our study since they allow one to draw a line between pseudocompressible and fully compressible regimes in the context of shock tube flows. We note that these conditions were approximately reached in the shock tube experiment of Poggi *et al.* [32], which is rather typical of this kind of experiment. Of course, not all shock tube experiments will fall within the range of application of the pseudocompressible approximation. In particular, the validity conditions (16) are compatible with a RDT regime as long as it remains moderate [Eq. (17)]. More intense RDT regimes involving acoustic phenomena may be encountered in shock tube applications: They are almost observed in the experiment of Poggi *et al.* [32].

Several consequences of the pseudocompressible approximation on turbulence modeling have also been put forth. Production terms in the density variance and flux equations as well as the turbulent transport of energy can be made compatible with pseudocompressible results.

The results have been validated by means of comparisons with a numerical simulation, performed with the TRICLADE code, of the interaction of a rarefaction wave with a turbulent mixing zone. They are of practical interest for turbulence modeling of stably or unstably stratified compressible turbulent mixtures, such as those found in geophysical flows, engine combustion, supernova explosions, or inertial confinement fusion experiments.

APPENDIX: GRADIENT JUMPS AT THE RAREFACTION HEAD

The rarefaction head is a weak discontinuity in the sense that the primitive variables are continuous but their longitudinal gradients jump across it. Assuming weak perturbations, linearization of the equations allows one to get some insight into the interaction of the rarefaction head with an upstream weak turbulence.

The fluctuations of the primitive variables and also their transverse derivatives are continuous across the rarefaction head. The jump of the longitudinal derivative of the transverse velocity is decoupled from the other jumps and related only to the front corrugation. The system for the jumps of the other longitudinal derivatives can be solved up to an arbitrary constant C. Let us denote by x the longitudinal direction, by x_{RH} the location of the rarefaction head, and by $\bar{a}$ the local mean sound speed. For a left-facing rarefaction, denoting by $[\![g]\!] = g(x_{\mathrm{RH}}^+) - g(x_{\mathrm{RH}}^-)$ the jump of g across the rarefaction head (with the value inside minus the value outside the rarefaction) and defining

$$w_a^+ = \frac{p'}{\bar{\rho}\bar{a}^2} + \frac{u'}{\bar{a}}, \quad w_a^- = \frac{p'}{\bar{\rho}\bar{a}^2} - \frac{u'}{\bar{a}}, \quad w_s = \frac{p'}{\bar{\rho}\bar{a}^2} - \frac{\rho'}{\bar{\rho}},$$

the following result can be obtained:

$$\begin{pmatrix} [\![\partial_x w_s]\!] \\ [\![\partial_x w_a^+]\!] \\ [\![\partial_x w_a^-]\!] \end{pmatrix} = \frac{1}{\gamma-1}\frac{\partial_x \bar{a}}{\bar{a}}(x_{\mathrm{RH}}^+) \times \begin{pmatrix} \frac{2\gamma'}{\gamma} \\ -\frac{p'}{\bar{P}} + \frac{\rho'}{\bar{\rho}} - (\gamma-1)\frac{u'}{\bar{a}} + \frac{\gamma'}{\gamma} \\ -3\frac{p'}{\bar{P}} - \frac{\rho'}{\bar{\rho}} + (\gamma-1)\frac{u'}{\bar{a}} - \frac{\gamma'}{\gamma} + 4C \end{pmatrix}_{(x_{\mathrm{RH}})}. \quad \text{(A1)}$$

For the one-dimensional case, the quantities w_a^+ and w_a^- respectively correspond to the downstream and upstream propagating characteristics. For a single gas case, the quantity w_s is an entropy wave and its gradient is continuous across the rarefaction front. If the upstream weak turbulent field is assumed to be known, then $[\![\partial_x w_s]\!]$ and $[\![\partial_x w_a^+]\!]$ are also known from Eq. (A1) and shown to scale with the sound speed gradient just downstream from x_{RH}. This implies that the jumps decrease as the rarefaction extension grows.

It is well known that no wave can propagate from inside the rarefaction to the head. However, the w_a^- waves travel at the same speed as the rarefaction and the w_a^+ and w_s waves acts as source terms for w_a^- inside the rarefaction. That is why the value of the constant C depends on the whole history of the rarefaction. At x_{RH}, the evolution equation for w_a^- is an ordinary differential equation and not a partial differential equation. It can be solved if the upstream field is known, but many assumptions are required to get closed solutions.

The important point with respect to the validity of the pseudocompressible approximation developed in this paper is that the fluctuating velocity divergence jumps across the rarefaction head and becomes immediately nonzero even if the upstream field is divergence-free.

[1] D. R. Durran, J. Atmos. Sci. **46**, 1453 (1989).
[2] N. Botta, R. Klein, and A. Almgren, Potsdam Institut fur Klimafolgenforschung Report No. PIK 55, 1999 (unpublished).
[3] A. Shirgaonkar and S. Lele, Phys. Fluids **18**, 066601 (2006).
[4] J. de Charentenay, Ph.D. thesis, École Centrale de Paris, 2001.
[5] A. S. Almgren, J. B. Bell, C. A. Rendleman, and M. Zingale, Astrophys. J. **637**, 922 (2006).
[6] A. S. Almgren, J. B. Bell, C. A. Rendleman, and M. Zingale, Astrophys. J. **649**, 927 (2006).
[7] A. S. Almgren, J. B. Bell, C. A. Rendleman, and M. Zingale, Astrophys. J. **684**, 449 (2008).
[8] J. Sanz, L. Masse, and P. Clavin, Phys. Plasmas **13**, 102702 (2006).
[9] B. Launder, B. Reece, and W. Rodi, J. Fluid Mech. **68**, 537 (1975).
[10] V. R. Kuznetsov and V. A. Sabel'nikov, *Turbulence and Combustion* (Hemisphere, London, 1990).
[11] S. B. Pope, Prog. Energy Combust. **27**, 119 (1985).
[12] R. M. C. So, C. Y. Zhao, and T. B. Gatski, Flow Turb. Comb. **63**, 193 (1999).
[13] Y. Shimomura, Phys. Fluids **11**, 3136 (1999).
[14] L. Mathelin, F. Bataille, and Y. Zhou, Theor. Comput. Fluid Dyn. **22**, 471 (2008).
[15] R. Schiestel, *Modeling and Simulation of Turbulent Flows* (Wiley, New York, 2008).
[16] V. A. Andronov, S. M. Bakhrakh, E. E. Meshkov, V. N. Mokhov, V. V. Nikiforov, A. V. Pevnitskii, and A. I. Tolshmyakov, Sov. Phys. JETP **44**, 424 (1976).
[17] S. H. Fergason, T. L. Ho, B. M. Argrow, and G. Emanuel, J. Fluid Mech. **445**, 37 (2001).
[18] J. C. R. Hunt and D. J. Carruthers, J. Fluid Mech. **212**, 497 (1990).
[19] L. Jacquin, C. Cambon, and E. Blin, Phys. Fluids A **5**, 2539 (1993).
[20] W. D. Thacker, S. Sarkar, and T. B. Gatski, Theor. Comput. Fluid Dyn. **21**, 171 (2007).
[21] H. Yu and S. S. Girimaji, Phys. Fluids **19**, 041702 (2007).
[22] S. Sarkar, Phys. Fluids A **4**, 2674 (1992).
[23] O. Grégoire, D. Souffland, and S. Gauthier, J. Turbulence **6**, 1 (2005).
[24] A. Banerjee, R. A. Gore, and M. J. Andrews, Phys. Rev. E **82**, 046309 (2010).
[25] D. Besnard, J.-F. Haas, and R. M. Rauenzahn, Physica D **37**, 227 (1989).
[26] V. Andronov, S. M. Bakhrakh, E. E. Meshkov, V. V. Nikiforov, A. V. Pevnitskii, and A. I. Tolshmyakov, Sov. Phys. Dokl. **27**, 393 (1982).
[27] V. Giovangigli, *Multicomponent Flow Modeling* (Birkhääuser, Boston, 1999).
[28] D. Mihalas and B. W. Mihalas, *Foundations of Radiation Hydrodynamics* (Dover, New York, 2000).
[29] R. P. Drake, *High-Energy-Density Physics* (Springer, New York, 2006).
[30] H. Hanazaki and J. C. R. Hunt, J. Fluid Mech. **318**, 303 (1996).
[31] Y. Zhou, Phys. Rep. **488**, 1 (2010).
[32] F. Poggi, M. H. Thorembey, and G. Rodriguez, Phys. Fluids **10**, 2698 (1998).
[33] Y. Zhou, H. F. Robey, and A. C. Buckingham, Phys. Rev. E **67**, 056305 (2003).
[34] P. Chassaing, R. A. Antonia, F. Anselmet, L. Joly, and S. Sarkar, *Variable Density Fluid Turbulence* (Kluwer, Dordrecht, 2002).
[35] V. Daru and C. Tenaud, J. Comput. Phys. **193**, 563 (2004).
[36] J. Griffond, Phys. Fluids **18**, 4106 (2006).
[37] J. Griffond, O. Soulard, and D. Souffland, Phys. Scr. T **142**, 014059 (2010).
[38] B. Thornber, D. Drikakis, D. L. Youngs, and R. J. R. Williams, J. Fluid Mech. **654**, 99 (2010).